

Minimizing the grid-resolution dependence of flow-routing algorithms for geomorphic applications

Jon D. Pelletier

Department of Geosciences, University of Arizona, 1040 East Fourth Street, Tucson, AZ 85721-0077, USA

ARTICLE INFO

Article history:

Received 16 February 2010

Received in revised form 20 May 2010

Accepted 2 June 2010

Available online 8 June 2010

Keywords:

Numerical modeling

Flow routing

Fluvial processes

Raster-based algorithms

ABSTRACT

The results of flow-routing methods currently used in the geomorphic literature depend on grid resolution. This poses a problem for landscape evolution models, which must be independent of grid resolution to the greatest extent possible. Here I illustrate a refinement of currently-used flow-routing algorithms that yields unit contributing areas (i.e. contributing areas per unit width of flow) with minimal grid-resolution effects. I illustrate the application of this method in idealized topography, in high-resolution Digital Elevation Models (DEMs) of real-world topography, and by integration into a landscape evolution model for ridge-and-valley topography. The landscape evolution model produces grid-resolution-independent results in a more straightforward way than previous models for this type of landscape.

© 2010 Elsevier B.V. All rights reserved.

1. Introduction

Fluvial landscape evolution models require the calculation of contributing area, a proxy for discharge. The three most commonly used methods for calculating contributing area are D8 (O'Callaghan and Mark, 1984), MFD (Freeman, 1991; Quinn et al., 1991), and D^∞ (Tarboton, 1997). The D8 method routes flow from each pixel towards the neighboring pixel (including diagonals) that represents the steepest descent. D8 has the widely-recognized problem that flow pathways are unrealistically restricted to multiples of 45° . The MFD and D^∞ methods were designed to avoid this problem, i.e. they provide more flexibility by allowing flow to be partitioned among multiple downslope neighbors. The MFD method works by partitioning flow between each pixel and its downslope neighboring pixels by an amount related to the slope in the direction of each downslope neighbor. The D^∞ method partitions flow between two adjacent neighboring pixels whose triangular facet (formed by intersection with the center pixel) represents the steepest descent. The MFD method works best in planar or convergent topography while the D^∞ method works best in planar or convergent topography based on benchmark calculations of Tarboton (1997).

Both the MFD and D^∞ flow-routing methods suffer from an important problem, however: they are grid-resolution dependent. This grid-resolution dependence has been widely documented in the hydrologic (e.g. Wolock and McCabe, 1995), glaciologic (e.g. Le Brocq et al., 2006), and geomorphic (e.g. Schoorl et al., 2000) literatures but solutions to this problem are needed. Fig. 1A schematically compares the results of flow routing on Digital Elevation Models (DEMs)

representing planar and convergent hillslopes. On a planar hillslope, flow is routed in the direction of the slope aspect, assumed here to be parallel to one of the cardinal directions. The contributing area of each pixel at the slope base is, therefore, equal to $L\delta$, where L is the slope length and δ is the pixel width. At the outlet of the convergent slope (the point to which all flow is routed in this hypothetical example), the contributing area is equal to L^2 . As such, the contributing areas of pixels on planar hillslopes depend on pixel width while the contributing areas of pixels in zones of strongly convergent flow (where all flow is focused into a pathway narrower than a pixel width) do not depend on pixel width. Fig. 1C,D illustrates the ratios of contributing areas calculated by the MFD and D^∞ methods on a synthetic second-order drainage basin (illustrated in Fig. 1B) with pixel width δ to the contributing area of the same drainage basin whose topography is bilinearly interpolated to a pixel width $\delta/2$ (shown here for $\delta=0.25$ m). In this analysis, the contributing areas computed on the interpolated grid are subsampled to the same resolution as the original grid, adopting the maximum value for contributing area within the 2×2 pixel subdomains of the interpolated DEM that represent each pixel in the original DEM. In order for a flow-routing algorithm to be grid-resolution independent, the ratios of the contributing areas calculated with pixel width δ to the contributing areas of the exact same DEM interpolated to a pixel width $\delta/2$ and then subsampled back to the original pixel width should be 1 or nearly 1 everywhere on the landscape. The fact that these ratios differ significantly from 1 (i.e. they are between 1.2 and 2 on hillslopes and close to 1 in the pixels that comprise the tributary valley network) indicates that the MFD and D^∞ methods are grid-resolution dependent. This is a general problem for any value of δ and for any landscape that includes hillslopes of variable convergence and/or both hillslopes and valleys. This problem is not solved by simply dividing the contributing

E-mail address: jdpellet@email.arizona.edu.

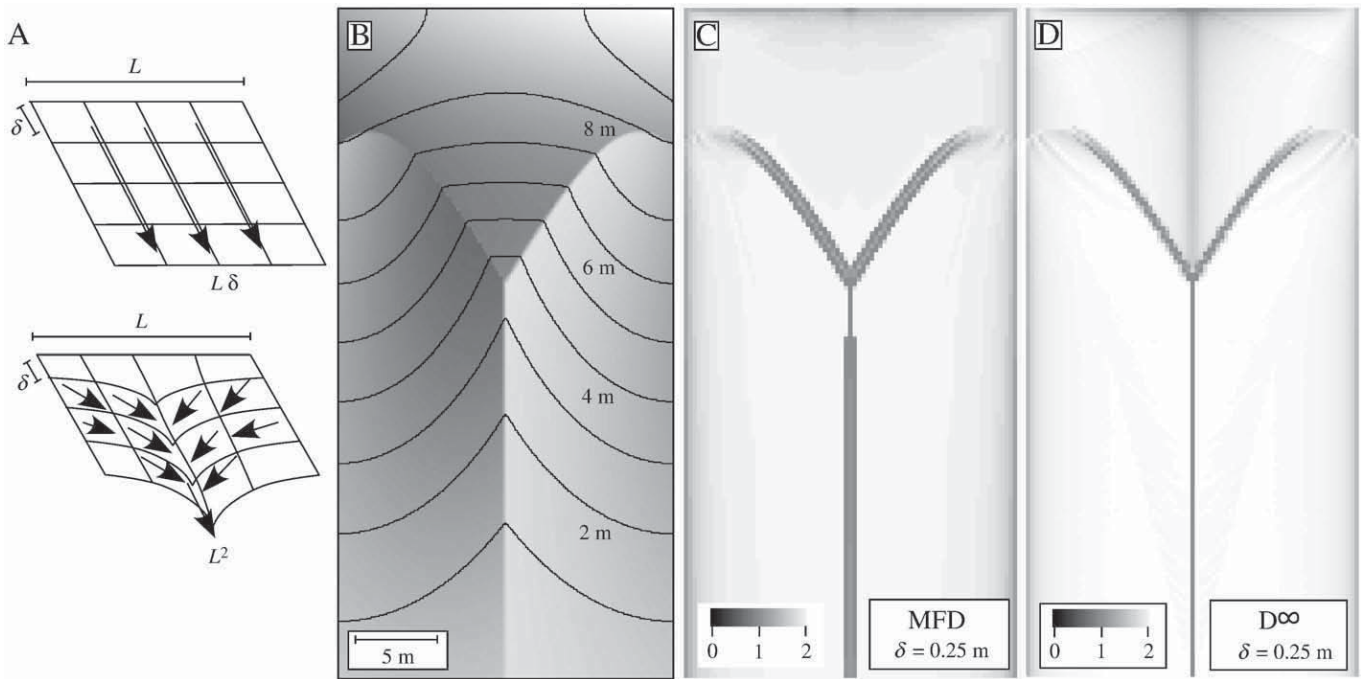


Fig. 1. Dependence of flow-routing methods on grid resolution. (A) Schematic illustration of flow in planar (top) and convergent (bottom) hillslopes. On planar hillslopes, contributing areas at the slope base are equal to $L\delta$, where δ is the pixel width, while in convergent hillslopes it is L^2 . (B) Shaded-relief and contour map of synthetic second-order drainage basin. (C–D) Ratios of contributing areas calculated with pixel width δ to the contributing areas of the same topography bilinearly interpolated to a pixel width $\delta/2$ (shown here for $\delta = 0.25$ m) for (C) the MFD method and (D) the D^∞ method. Note that although values in this map range from 1 to 2, the scale ranges from 0 to 2 in order to facilitate comparison with later figures.

areas by the pixel width to obtain unit contributing areas, because then the unit contributing areas of the tributary valley network will depend on pixel width. Moreover, the ratios of contributing areas calculated in DEMs of different resolutions are not precisely equal to the ratio of pixel widths even on hillslopes. As illustrated in Fig. 1C,D, the ratio varies from 1.2 to 2 depending on the degree of convergence, the distance from the divide, and the flow-routing method used. To solve this problem, a modification of the MFD and D^∞ methods is needed.

Before I describe such a modification, it is important to note that landscape evolution models actually require unit or specific contributing area, i.e. the contributing area per unit width of flow in the dominant fluvial pathway within each pixel, not contributing area itself. As such, my goal in this paper is to present a method that minimizes the grid-resolution dependence in the computation of unit contributing area. Landform evolution models of regolith-covered landscapes in which fluvial erosion rates are assumed to be a power-law function of unit stream power, for example, have the form

$$\begin{aligned} \frac{\partial z}{\partial t} &= \frac{\rho_r}{\rho_s} U - K \left(\left(\frac{A}{w} \right)^p S^n - \theta_c \right) & \text{if } \left(\frac{A}{w} \right)^p S^n > \theta_c \\ &= \frac{\rho_r}{\rho_s} U & \text{if } \left(\frac{A}{w} \right)^p S^n \leq \theta_c \end{aligned} \quad (1)$$

where z is elevation, t is time, ρ_r is the rock density, ρ_s is the regolith density, U is the rock uplift rate, K is an erodibility coefficient dependent on climate and substrate erodibility, A is the contributing area, w is the width of flow in the dominant fluvial pathway of each pixel, S is the bed slope, p and n are dimensionless coefficients, and θ_c is the detachment threshold below which no erosion takes place. Colluvial erosion/deposition has been neglected in Eq. (1) (to focus the discussion on fluvial erosion rates) but will be added in Section 3. Proper application of Eq. (1) requires that the width of flow, w , in the dominant fluvial pathway of each pixel be calculated, taking into account differences in the widths of flow between hillslope pixels and tributary valley pixels. Distinguishing between hillslope and tributary

valley pixels in the calculation of flow width is important for two reasons. First, while flow in tributary valley pixels occurs in a single dominant channel, flow on hillslopes may be unconfined (e.g. no channels or rills are present) or distributed among several finely-spaced channels, rills, or microtopographically-generated zones of concentrated overland flow. Second, in order to calculate a unit contributing area in Eq. (1) that is independent of pixel width, it is necessary for the width of flow in hillslope pixels to scale with pixel width, since the contributing area in hillslope pixels scales with pixel width and the unit contributing area is the ratio of contributing area to width. Conversely, the width of flow in tributary valley pixels must not depend on pixel width because contributing area does not depend on pixel width. By quantifying fluvial erosion rates using the ratio of contributing area to flow width and distinguishing between flow widths in hillslope and tributary valley pixels, fluvial erosion rates independent of grid resolution can be calculated.

In tributary valleys, each pixel contains one dominant channel and it is often a good approximation to assume that the width of flow in that channel is proportional to a power function of the contributing area, i.e.

$$w_v = cA^b \quad (2)$$

where $b \approx 1/2$ and c is a coefficient that varies between drainage basins (Leopold and Maddock, 1953). If one assumes that Eq. (2) applies to all pixels (both hillslope and valley) and substitutes Eq. (2) into Eq. (1), subsuming the coefficient c into K and θ_c , one obtains the familiar form of the stream-power erosion model for regolith-covered landscapes (Howard, 1994; Perron et al., 2008, 2009):

$$\begin{aligned} \frac{\partial z}{\partial t} &= \frac{\rho_r}{\rho_s} U - K (A^m S^n - \theta_c) & \text{if } A^m S^n > \theta_c \\ &= \frac{\rho_r}{\rho_s} U & \text{if } A^m S^n \leq \theta_c \end{aligned} \quad (3)$$

where $m = p - b$. If $p = 1$ and $b = 1/2$, for example, $m = 1/2$. Eqs. (1)–(3) illustrates that the stream-power model can be formulated in terms of unit contributing area A/w rather than A . The formulation based on A/w (i.e. Eq. (1)) is more fundamental than the formulation based on A (i.e. Eq. (3)) because Eq. (1) does not assume that the power-law relationship between contributing area and flow width (i.e. Eq. (2)) applicable to tributary valleys is also applicable to hillslopes. On hillslopes, the width of flow in each pixel is equal to the pixel width, i.e. $w_h = \delta$, if flow occurs as sheetflooding. Alternatively, if flow occurs in rills or microtopographically-generated zones of concentrated overland flow, the width of flow is equal to some fraction of a pixel width, e.g. $w_h = (w_r/\lambda_r)\delta$, where w_r is the width of flow in each rill or zone of concentrated flow and λ_r is the mean rill/zone spacing. Values of the proportionality between w_h and δ in cases where hillslopes are rilled or where concentrated overland flow occurs must be constrained using site-specific data for the fraction of hillslope area subject to fluvial erosion during high-magnitude storm events. For example, on rilled hillslopes, field measurements of rill width and spacing may be used to constrain w_r/λ_r . This value can be expected to depend sensitively on hillslope microtopography, however, and more research is needed on how to best constrain this ratio.

When modeling the development of large drainage basins over geologic time scales, it is often computationally unfeasible to resolve low-order channels in cross section. In such cases, which are the focus of this paper, the variable z in Eq. (1) can be assumed to represent the average elevation within an area δ^2 or the elevation of a point along the dominant fluvial pathway (which may be a channel, a series of rills, or a hillslope segment subject to sheetflooding) within each pixel. In this paper I argue that the stream-power model is most accurately applied and that grid-resolution effects are minimized when z in Eq. (1) represents the elevation values at *points* along the dominant fluvial pathway within each pixel rather than representing the average elevation within *areas* of each pixel. This distinction is important for devising optimal strategies for minimizing grid-resolution effects in landscape evolution models. Assuming that z represents the average elevation within an area of each pixel has the disadvantage that the slope term in Eq. (1) does not equal the along-channel slope required by the stream-power model. Instead, the slope term corresponds to the derivative of the average elevation of each pixel, including both valleys and their adjacent sideslopes. The slope calculated in this way is likely to be larger than the actual along-channel slope, especially in narrow, low-order valleys, because such valleys are flanked by steeper sideslopes that can bias the slope towards larger values. More broadly, the assumption that z represents the average elevation within a pixel is difficult to reconcile with observed slope–area relationships. Howard (1994) and Perron et al. (2008, 2009), for example, advocate scaling the fluvial erosion rate by the ratio of the channel width to the pixel width based on the assumption that z represents the average elevation within each pixel and all pixels have one channel. Scaling the fluvial erosion rate in this way yields

$$E = \frac{w}{\delta} K A^m S^n \propto \frac{K}{\delta} A^{m+1/2} S^n \quad (4)$$

where E is the fluvial erosion rate, assuming $A^m S^n \gg \theta_c$ (i.e. in valleys far from valley heads) and $w \propto A^{1/2}$. In topographic steady state, Eq. (4) predicts $S \propto A^{-(m+1/2)/n}$. Observed valley slope–area relationships generally follow a power-law relationship with exponents of between -0.35 and -0.6 (Whipple and Tucker, 1999; Stock and Montgomery, 1999). If $n = 1$ is assumed in Eq. (4), slope–area relationships for valley channels in topographic steady state, therefore, imply values for m in the range of -0.15 to 0.1 . Such values are unrealistically low. The value of n is not precisely constrained, but studies where n has been calibrated in real-world landscapes (e.g. Howard and Kerby, 1983) have generally concluded that n is less than or equal to 1. Perron et al. (2008) avoid

this discrepancy between observed slope–area relationships and those predicted by their model by assuming channels have uniform width in this step of their analysis (i.e. $w_h = w_v = 1$ in paragraph 23 of Perron et al., 2008).

2. Flow-routing methods that minimize grid-resolution dependence

One approach to minimizing the grid-resolution dependence of flow-routing methods is to use the “error” maps in Fig. 1 as input to a “correction” step. In this approach, a flow-routing algorithm (e.g. MFD and D^∞) is first applied to the landscape to compute contributing areas. Then, the flow-routing method is applied to the same topography bilinearly interpolated to have a pixel width equal to one half of the original grid, as in the analysis presented in Fig. 1C,D. The contributing area grid computed from the interpolated DEM is then subsampled to the same resolution as the original DEM, adopting the maximum value for contributing area within the 2×2 pixel subdomains of the interpolated DEM that represent each pixel in the original DEM. The maximum value within each subdomain is chosen because the goal is to quantify the fluvial erosion rate of the dominant fluvial pathway within each pixel. The ratio of these two contributing area maps is then computed and denoted as f . The unit contributing area, a , is then calculated as

$$a = \begin{cases} \frac{A}{w_h} & \text{if } f \geq 1.2 \\ \frac{A}{w_v} & \text{if } f < 1.2 \end{cases} \quad (5)$$

where w_h is the flow width on hillslopes (i.e. $w_h = \delta$ if flow occurs as sheetflooding and $w_h = (w_r/\lambda_r)\delta$ if flow occurs in rills or zones of concentrated overland flow) and w_v is given by Eq. (2). This approach exploits the fact that the values of f differ on hillslopes (i.e. varying from approximately 1.2 to 2 depending on the degree of convergence) and in valleys (i.e. nearly equal to 1) in order to normalize the contributing area by the appropriate value of the width of the flow in each type of pixel (hillslope or valley). Results obtained with the synthetic landscape of Fig. 1B suggest that a cutoff value of 1.2 works best for distinguishing between hillslope and valley pixels, i.e. if the cutoff value is set significantly lower than 1.2, portions of first-order valleys are misidentified as hillslopes; while if the value is set significantly higher than 1.2, portions of convergent hillslopes are misidentified as valleys. The value of the cutoff used in Eq. (5) ultimately must reproduce the transition between tributary channels (in valleys) and unchanneled or rilled topography (on hillslopes) in a given landscape. Where this transition occurs in relationship to the degree of convergence of the larger, pixel-scale topography that controls f may vary from one landscape to the next. As such, the cutoff value in Eq. (5) is not unique, but 1.2 represents a useful default value.

The results of Eq. (5) on the synthetic landscape of Fig. 1B are illustrated in Figs. 2 and 3 for the MFD and D^∞ methods, respectively. Figs. 2A,B and 3A,B illustrate the unit contributing area, a , of this landscape calculated with $\delta = 0.5$ and $\delta = 0.25$ m. Relatively high values of a occur in the first and second-order valleys of the landscape (where a is also controlled by the values of b and c in Eq. (2), here assumed to be 1/2 and 0.001, respectively, i.e. the channel width increases as the square root of contributing area with a reference value of $w_v = 0.1$ m for $A = 0.01$ km²). Lower values of a occur in the adjacent hillslopes, where flow is assumed to occur as sheetflooding (i.e. $w_h = \delta$) in this example. Figs. 2C,D and 3C,D illustrate the ratios of unit contributing areas calculated using pixel widths of δ and $\delta/2$ for two different values of δ . As in the analysis illustrated in Fig. 1C,D, the unit contributing areas calculated using pixel width $\delta/2$ are subsampled to match the resolution of the grid with pixel width δ , adopting the maximum value within each 2×2 pixel subdomain in the subsampling. A comparison of Figs. 2C,D and 3C,D with 1C,D

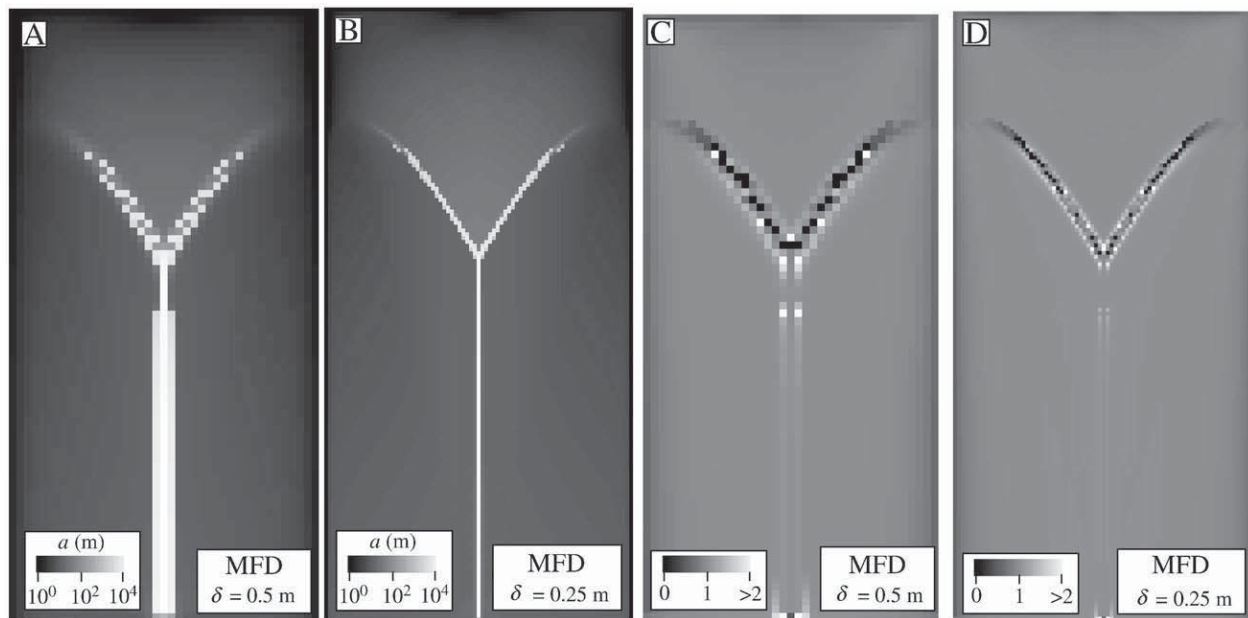


Fig. 2. Results of the MFD method with scale correction (Eq. (5)) applied to the synthetic second-order drainage basin of Fig. 1B. (A–B) Unit contributing areas, a , of the synthetic landscape of Fig. 1B with value of c (the coefficient in the width–area scaling in valleys) assumed equal to 0.001 and a pixel width of (A) $\delta = 0.5$ m and (B) $\delta = 0.25$ m. (C–D) Ratios of the unit contributing areas, a , calculated using a pixel width δ to the unit contributing areas of the same landscape calculated with pixel width $\delta/2$, for (C) $\delta = 0.5$ m and (D) $\delta = 0.25$ m.

indicates that the correction step greatly reduces, but does not entirely eliminate, the grid-resolution dependence of these flow-routing methods. Values of a are nearly grid-resolution independent (i.e. the ratios illustrated in Figs. 2C,D and 3C,D are nearly 1) on hillslopes and in valleys with azimuths that are multiples of 45° (i.e. the second-order valley, which trends from top to bottom in this image). The correction method is less successful at eliminating the scale-dependence in portions of valleys that trend along other azimuths, such as in the first-order valleys of this landscape, which have azimuths of 150° and 210° . The ratios of unit contributing areas

in portions of these first-order valleys differ significantly from 1 (being both larger and smaller than 1). Because these flow-routing methods are grid-based, the discharge pathways along valleys with azimuths that differ from multiples of 45° are necessarily approximated by a series of segments that partition flow to neighbors that do trend along multiples of 45° . These discharge pathways depend on grid resolution in a way that is difficult to eliminate. Nevertheless, the correction step results in a significant improvement over the results of flow-routing methods with no correction step based on a visual comparison of Figs. 2C,D and 3C,D with Fig. 1C,D. There are also

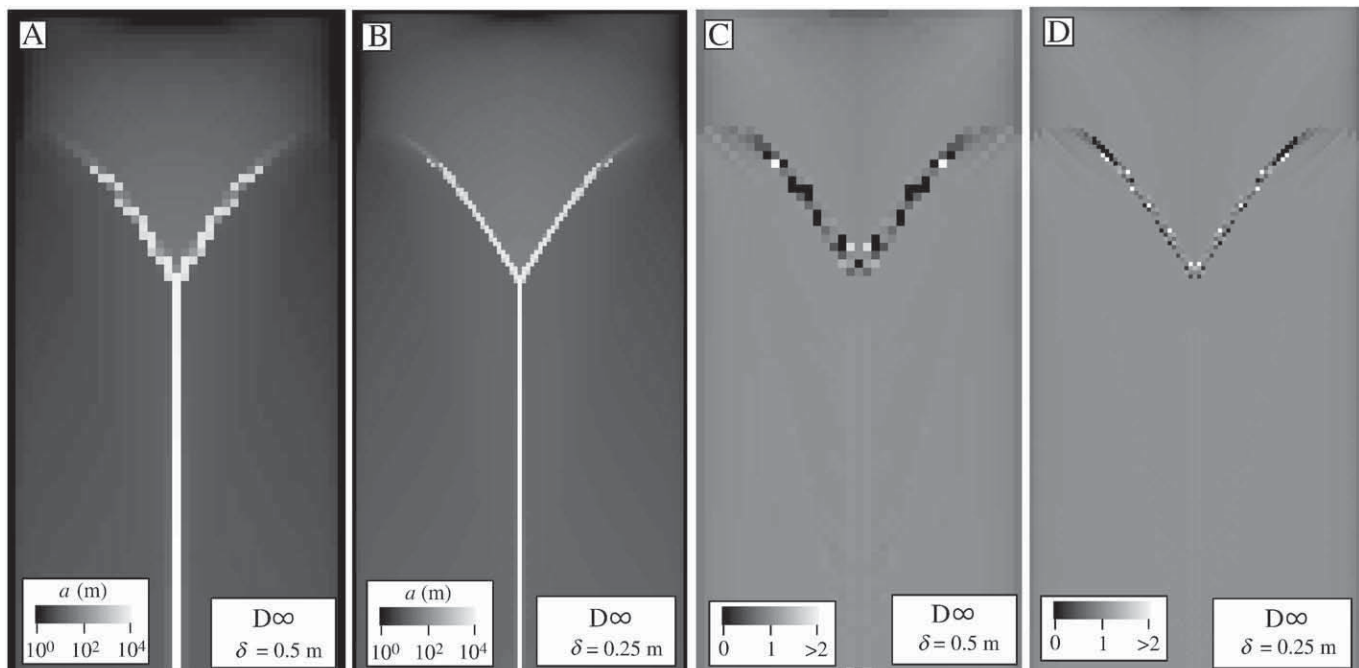


Fig. 3. Results of the D^∞ method with scale correction (Eq. (5)) applied to the synthetic second-order drainage basin of Fig. 1B. (A–D) Same as Fig. 2A–D, except that the D^∞ method is used instead of the MFD method.

significant differences in the efficacy of the correction step between the two underlying flow-routing methods. Using the MFD method, drainage along the second-order valley of this synthetic landscape occurs not just along the single pixel that represents the valley bottom, but also along neighboring pixels to the left and right of that line of pixels (Fig. 2A,B). The D^∞ method (Fig. 3A,B) does a better job of restricting the flow in that second-order valley (which is narrower than a pixel width, based on the assumption that valley-floor channels are not resolved in cross section) to a single line of pixels. It is important to note that although the channel may appear “wider” in the results obtained with larger pixel widths, the channel is not wider if the valley is restricted to a single line of pixels (as in the results of the D^∞ method), because, as noted above, the values of each quantity

represent values at a *point* within the dominant fluvial pathway of each pixel.

Fig. 4 illustrates the results of Eq. (5) to an actual ridge-and-valley landscape in the Walnut Gulch Experimental Watershed, southeastern Arizona, represented by a 1 m/pixel bare-ground DEM constructed from airborne LiDAR data (Fig. 4A). I illustrate only the D^∞ method in this case because that is the preferred method for predominantly convergent topography based on the results of Tarboton (1997). Fig. 4B–D illustrate the unit contributing areas (Fig. 4B) and ratios of unit contributing areas calculated using pixel widths of δ and $\delta/2$ for two different values of δ (Fig. 4B,C). On hillslopes I assumed unconfined flow and in valleys I assumed Eq. (2) with $b = 1/2$ and $c = 0.01$ in this example. The 1 m/pixel LiDAR DEM

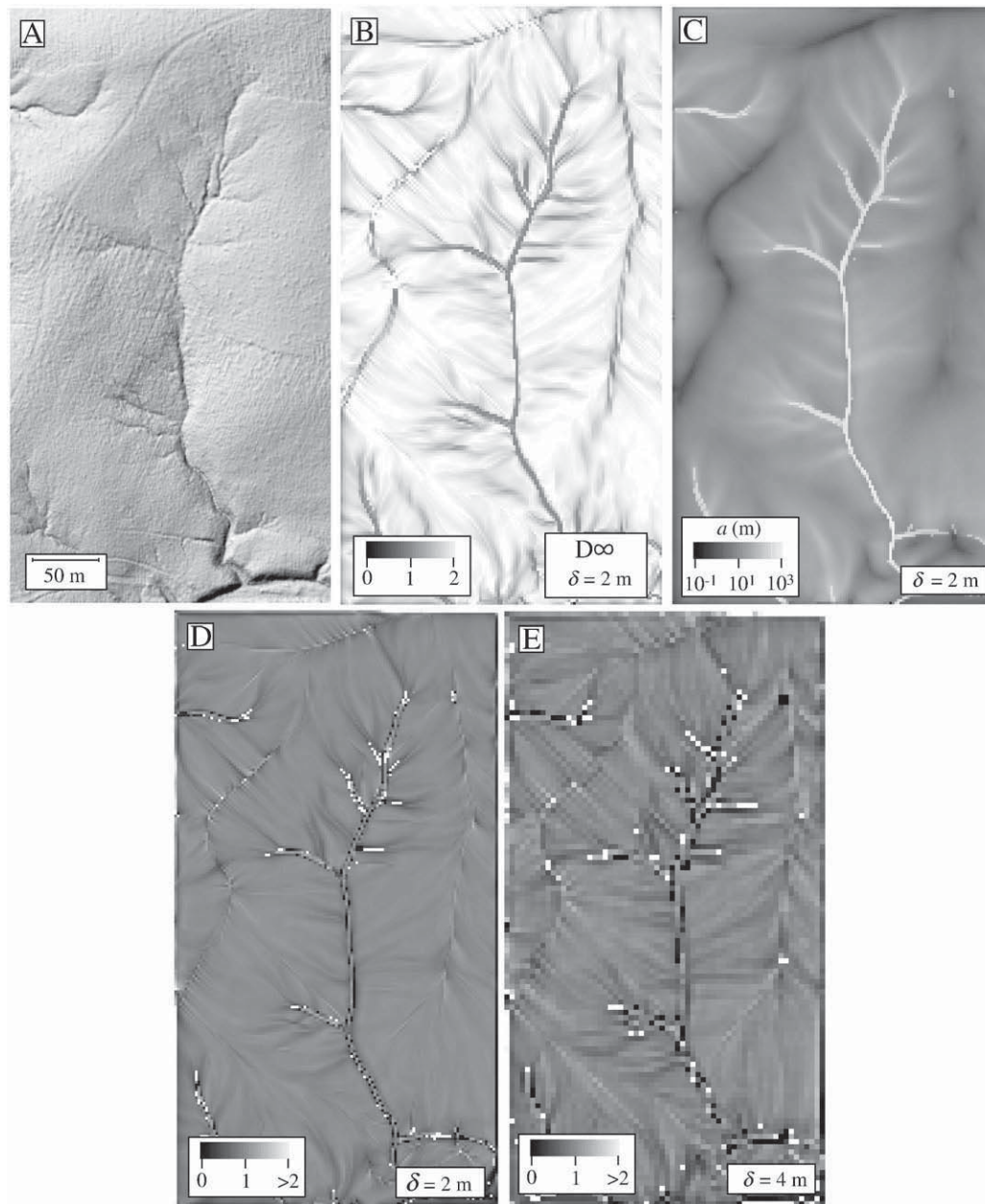


Fig. 4. Results of the D^∞ method with scale correction (Eq. (5)) applied to an actual ridge-and-valley landscape in the Walnut Gulch Experimental Watershed in southeastern Arizona. (A) 1 m/pixel bare-ground DEM of the landscape constructed from airborne LiDAR data. (B) Ratios of contributing areas calculated with pixel width δ to the contributing areas of the same topography bilinearly interpolated to a pixel width $\delta/2$ (shown here for $\delta = 2$ m). (C) Unit contributing areas, a , of the landscape of A with value of c (the coefficient in the width–area scaling in valleys) assumed equal to 0.01 and a pixel width of $\delta = 2$ m. (D–E) Ratios of the unit contributing areas calculated using a pixel width δ to the unit contributing area of the same landscape calculated with pixel width $\delta/2$, for (C) $\delta = 2$ m and (D) $\delta = 4$ m.

was first smoothed by applying the diffusion equation with a diffusivity of $1 \text{ m}^2 \text{ kyr}^{-1}$ for 10 kyr. This type of preprocessing is needed when applying Eq. (5) to LiDAR DEMs because, without smoothing, the small-scale, artificial “noise” and striping in the DEM apparent in Fig. 4A causes artificial flow patterns on hillslopes. After smoothing, the DEM was subsampled in factors of two to create DEMs of $\delta = 2$ and 4 m. To create Fig. 4C, the ratios of unit contributing areas were calculated for the 1 m/pixel and 2 m/pixel DEMs, then the unit contributing area grid for the 1 m/pixel DEM was subsampled over 2×2 pixel subdomains, as in the analysis presented in Figs. 2C,D and 3C,D. The results for this real-world landscape are similar to those for the synthetic landscape of Fig. 1B illustrated in Figs. 2 and 3, i.e. unit contributing areas are nearly grid-resolution independent (i.e. the ratios illustrated in Fig. 4C,D are nearly 1) on hillslopes and in valley segments with an azimuth that is a multiple of 45° . Overall, the method greatly reduces the grid-resolution dependence of flow-routing methods in both idealized and real-world topography.

3. Integration into a landscape evolution model for the development of ridge-and-valley topography

In this section I combine the fluvial erosion rates calculated in Eq. (1) with hillslope diffusion to yield a model for the development of ridge-and-valley topography, following Howard (1994) and Perron et al. (2008, 2009). Sediment transport on vegetated or partially-vegetated hillslopes is often dominated by creep and bioturbation. The classic approach to modeling the evolution of relatively low-gradient hillslopes dominated by those processes is the diffusion equation (Culling, 1960, 1963):

$$\frac{\partial z}{\partial t} = D \nabla^2 z \quad (6)$$

where D is the diffusivity. Howard (1994) and Perron et al. (2008, 2009) demonstrated that the drainage density and spacing of first-order valleys in regolith-covered landscapes are controlled by the ratio of the rates of hillslope processes, modeled using Eq. (6), to fluvial processes, modeled using the stream-power model (i.e. Eq. (3),

assuming that the eroded regolith is transported predominantly as suspended load). The purpose of this section is not to reinvestigate the questions posed by Howard (1994) and Perron et al. (2008, 2009), but merely to show that the correction step described in the previous section can be used to construct landscape evolution model results that minimize grid-resolution dependence.

In order to combine hillslope diffusion and fluvial erosion within a framework in which z represents the elevation of the dominant fluvial pathway within each pixel, it is necessary to scale the rate of erosion/deposition from hillslope processes by the ratio δ/w for models with grids sufficiently coarse that channels are not explicitly resolved in cross section (as assumed here). On hillslopes with unconfined flow, the ratio δ/w is 1, hence the rate of erosion or deposition by hillslope processes is unaffected by this scaling. In valleys, however, the rate of deposition that occurs in the dominant fluvial pathway within each pixel is systematically underpredicted because the fluvial pathway is not resolved in cross section. The cross-sectional curvature is equal to the difference in the gradient of the side slopes adjacent to the dominant fluvial pathway divided by the width of that pathway. In a grid in which the flow width is narrower than the pixel width, the curvature will, therefore, be underestimated by a factor of δ/w , assuming that the gradients of the side slopes are adequately resolved. As such, it is necessary to scale the curvature values by δ/w to predict the correct colluvial deposition rate within the dominant fluvial pathway of each pixel. As illustrated in Fig. 5, the curvature values adjusted in this way result in values nearly independent of pixel width.

Applying the δ/w scaling to Eq. (6) and combining it with Eq. (1) yields

$$\begin{aligned} \frac{\partial z}{\partial t} &= \frac{\rho_r}{\rho_s} U + \frac{\delta}{w} D \nabla^2 z - K(a^p S^n - \theta_c) \quad \text{if } a^p S^n > \theta_c \\ &= \frac{\rho_r}{\rho_s} U + \frac{\delta}{w} D \nabla^2 z \quad \text{if } a^p S^n \leq \theta_c \end{aligned} \quad (7)$$

The model results presented in this section solve Eq. (7), assuming $p = n = 1$ and an initially low-relief landscape with minor (0.1 m root-mean-squared) white-noise variations. Slope–area relationships (e.g.

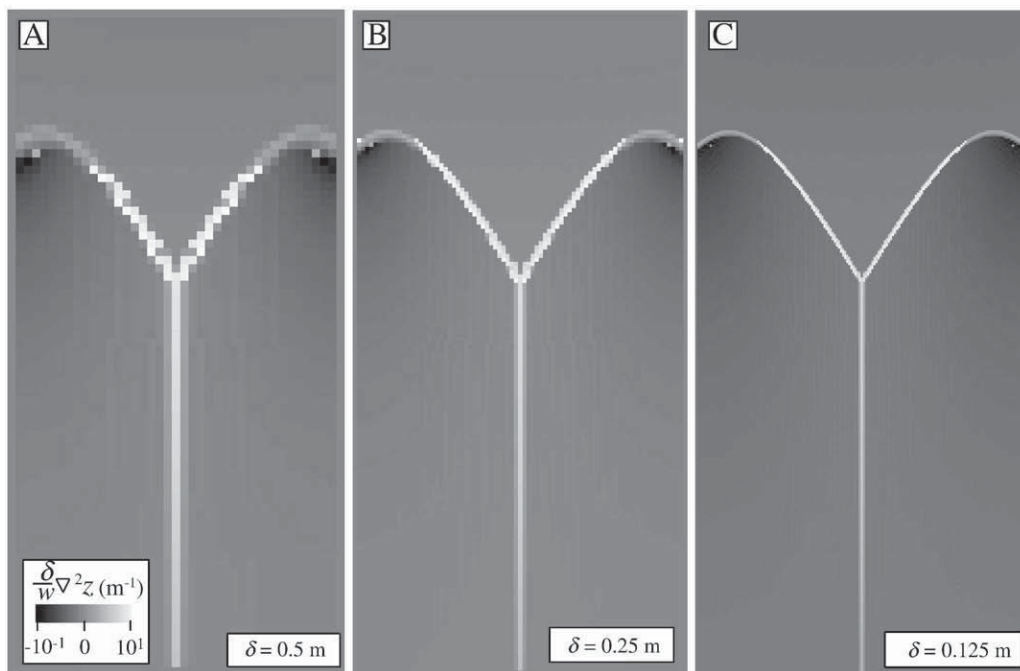


Fig. 5. Maps of the Laplacian scaled to the local flow width, $(\delta/w) \nabla^2 z$, for the synthetic landscape of Fig. 1B with $c = 0.001$, for (A) $\delta = 0.5$ m, (B) $\delta = 0.25$ m, and (C) $\delta = 0.125$ m. All images are shown with the same grayscale map. The similar tones in each map indicate that the rates of erosion/deposition computed by the diffusive portion of the model are nearly identical for a range of pixel widths if the Laplacian, $\nabla^2 z$, is scale-corrected via multiplication by δ/w .

$S \propto A^{-m/n}$ with m/n in the range of 0.35 to 0.60) imply p/n is in the range of 0.7 to 1.2 if $w_v \propto A^{1/2}$. The fluvial erosion component of Eq. (7) is solved for at each time step of the model by calculating S in the downslope direction using a time step that satisfies the Courant stability criterion. The diffusive component of Eq. (7) is calculated using an implicit numerical method that is stable for all time steps.

Fig. 6A–D illustrate the results of Eq. (7) on model domain 150×600 m driven by constant, uniform uplift for 5 Myr (i.e. until an approximate topographic steady-state condition was achieved). For these examples I used $(\rho_r/\rho_s)U = 0.1 \text{ m kyr}^{-1}$, $D = 3 \text{ m}^2 \text{ kyr}^{-1}$, $K = 0.005 \text{ kyr}^{-1}$, $c = 0.005$, and $\theta_c = 0$. As illustrated, the spacing of

first-order valleys predicted by the model is very similar as δ is varied from 0.625 to 5 m. The model does not produce precisely identical topography at different scales due to differing white-noise initial conditions. However, an average of ten simulations initiated with different microtopographic initial conditions at each pixel width yielded a mean valley spacing of 54 m for all values of δ , with a range of approximately 3 m within each set of ten runs of a given pixel width. The relief was 34.0 m with a range of 0.2 m for runs at different scales and initial conditions. Given that the component models for erosion/deposition by hillslope processes and erosion by fluvial processes separately yield results that are nearly grid-resolution

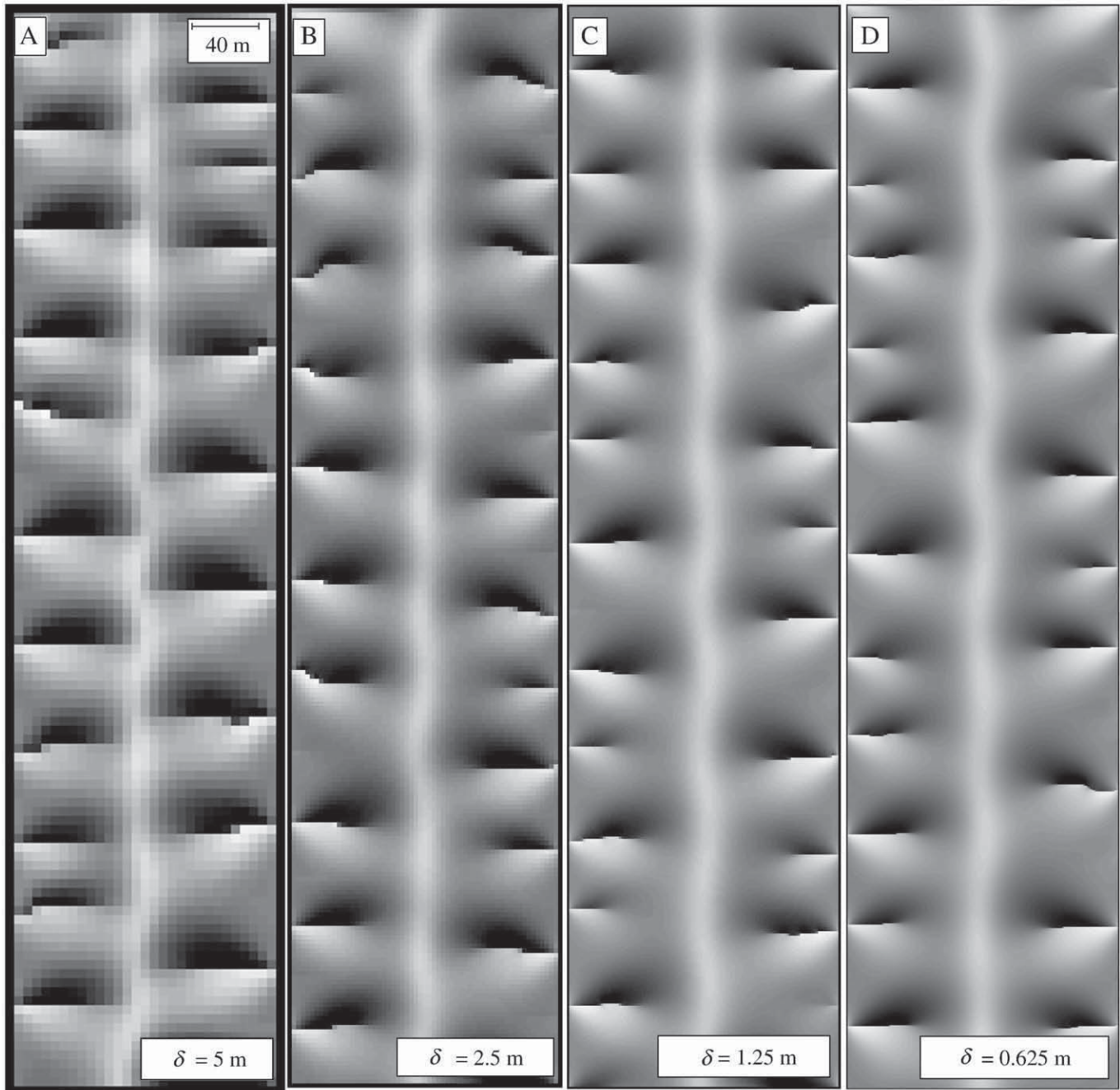


Fig. 6. Shaded-relief maps (illuminated from top to bottom) of results of the landscape evolution model (Eq. (7)) on a model domain 150×600 m driven by constant, uniform rock uplift for 5 Myr (i.e. until an approximate topographic steady-state condition was achieved). Model parameters include $(\rho_r/\rho_s)U = 0.1 \text{ m kyr}^{-1}$, $D = 3 \text{ m}^2 \text{ kyr}^{-1}$, $K = 0.005 \text{ kyr}^{-1}$, $c = 0.005$, and $\theta_c = 0$. Results vary between runs in terms of the specific valley positions (due to differences initial microtopography), but the average spacing between first-order valleys calculated from ten runs of each pixel size confirm the grid-resolution independence of the model.

independent, it is not surprising that a landform evolution model comprised of a combination of those two processes is also nearly grid-resolution independent.

4. Discussion and conclusions

It is useful to compare and contrast the method of this paper with other proposed methods for constructing grid-resolution-independent landscape evolution models of ridge-and-valley topography. The grid-resolution dependence of the D^∞ method documented in this paper is particularly relevant to the studies of Perron et al. (2008, 2009) because the location/spacing of valley heads is controlled, in part, by fluvial erosion rates at the junction between hillslopes (where the D^∞ depends on grid resolution) and tributary valleys (where it does not depend on grid resolution). Perron et al. (2008, 2009) were nonetheless able to achieve results independent of grid resolution by introducing two additional steps not used in this paper. First, they smoothed the contributing area grid by applying a moving-average filter prior to the calculation of fluvial erosion rates, as described in the supplementary information of Perron et al. (2009). Second, as noted in Section 1, they scaled fluvial erosion rates by the ratio of the channel width to the pixel width, assuming that the channel width is less than the pixel width. These steps are difficult to reconcile, however: the scaling step is based on the assumption that flow occurs in a channel that is narrower than the pixel width while the smoothing step forces flow to be distributed among multiple pixels. The smoothing step also introduces an additional length scale into the problem (greater than 10 m in the example case illustrated in Fig. S1 of Perron et al., 2009) that must be larger than any pixel width that might be used in the model. In this paper I advocate treating z as the elevation of a point along the dominant fluvial pathway within each pixel. Adopting this approach and computing the net erosion rate of each point in a grid-resolution-independent manner (e.g. by scaling the local curvature by the ratio of the pixel width to the local channel width, if diffusive processes are present) minimizes grid-resolution effects without the need to smooth or otherwise adjust the contributing area grid prior to the calculation of fluvial erosion rates.

This paper introduces a simple extension of widely-used flow-routing algorithms that minimizes the grid-resolution dependence of those algorithms. In this extension, the ratios of the contributing areas calculated for the same landscape at different scales are used to distinguish hillslopes from tributary valleys and calculate unit contributing areas that apply the appropriate flow width to each pixel type (i.e. hillslope or tributary valley). This method significantly reduces the grid-resolution dependence of two widely-used flow-routing methods (i.e. MFD and D^∞). The greatest limitation of the method is that it does not eliminate scale-dependence along valley segments that trend along azimuths that differ from multiples of 45° . Because flow-routing

methods are grid-based, the discharge pathways along such valleys are necessarily approximated by partitioning flow among a series of segments that trend along multiples of 45° . These discharge pathways depend on grid resolution in a way that is difficult to eliminate. Nevertheless, the method of this paper represents a significant advance as illustrated by its application in idealized topography, high-resolution DEMs of real-world topography, and by its integration into a landscape evolution model for the development of ridge-and-valley topography.

Acknowledgements

This study was partially funded by the Army Research Office project no. 55104-EV. I wish to thank Mark Nearing for sharing the Walnut Gulch LiDAR data with me and Phillippe Steer for helpful communications on grid-resolution effects in landform evolution models. I wish to thank Jack Schroder and an anonymous reviewer for their constructive comments.

References

- Culling, W.E.H., 1960. Analytical theory of erosion. *Journal of Geology* 68, 336–344.
- Culling, W.E.H., 1963. Soil creep and the development of hillside slopes. *Journal of Geology* 71, 127–161.
- Freeman, G.T., 1991. Calculating catchment area with divergent flow based on a rectangular grid. *Computers & Geosciences* 17, 413–422.
- Howard, A.D., 1994. A detachment-limited model of drainage basin evolution. *Water Resources Research* 30, 2261–2285.
- Howard, A.D., Kerby, G., 1983. Channel changes in badlands. *Geological Society of America Bulletin* 94, 739–752.
- Le Brocq, A.M., Payne, A.J., Siegert, M.J., 2006. West Antarctic balance calculations: impact of flux-routing algorithm, smoothing algorithm and topography. *Computers & Geosciences* 32, 1780–1795.
- Leopold, L.B., Maddock Jr., T., 1953. The Hydraulic Geometry of Stream Channels and Some Physiographic Implications. U.S. Geological Survey Professional Paper 252. 57 pp.
- O'Callaghan, J.F., Mark, D.M., 1984. The extraction of drainage networks from digital elevation data. *Computer Vision, Graphics, and Image Processing* 28, 323–344.
- Perron, J.T., Dietrich, W.E., Kirchner, J.W., 2008. Controls on the spacing of first-order valleys. *Journal of Geophysical Research* 113, F04016 doi: 10.1029/2007JF000977.
- Perron, J.T., Kirchner, J.W., Dietrich, W.E., 2009. Formation of evenly-spaced ridges and valleys. *Nature* 460, 502–505.
- Quinn, P.F., Beven, K.J., Chevallier, P., Planchon, O., 1991. The prediction of hillslope flow paths for distributed hydrological modeling using digital terrain models. *Hydrological Processes* 5, 59–79.
- Schoorl, J.M., Sonneveld, M.P.W., Veldkamp, A., 2000. Three-dimensional landscape process modelling: the effect of DEM resolution. *Earth Surface Processes and Landforms* 25, 1025–1034.
- Stock, J.D., Montgomery, D.R., 1999. Geologic constraints on bedrock river incision using the stream power law. *Journal of Geophysical Research* 104, 4983–4993.
- Tarboton, D.G., 1997. A new method for the determination of flow directions and upslope areas in grid Digital Elevation Models. *Water Resources Research* 33, 309–319.
- Whipple, K.X., Tucker, G.E., 1999. Dynamics of the stream-power river incision model: implications for the height limits of mountain ranges, landscape response timescales, and research needs. *Journal of Geophysical Research* 104, 17,661–17,674.
- Wolock, D.M., McCabe Jr., G.J., 1995. Comparison of single and multiple flow direction algorithms for computing topographic parameters in TOPMODEL. *Water Resources Research* 31, 1315–1324.